

Seeing is Understanding: Unlocking Causal Attention into Modality-Mutual Attention for Multimodal LLMs

Wei-Yao Wang* Zhao Wang Helen Suzuki Yoshiyuki Kobayashi
Sony Group Corporation, Tokyo, Japan
{wei-yao.wang, zhao.wang, helen.suzuki, yoshiyuki.kobayashi}@sony.com

Abstract

Recent Multimodal Large Language Models (MLLMs) have demonstrated significant progress in perceiving and reasoning over multimodal inquiries, ushering in a new research era for foundation models. However, vision-language misalignment in MLLMs has emerged as a critical challenge, where the textual responses generated by these models are not factually aligned with the given text-image inputs. Existing efforts to address vision-language misalignment have focused on developing specialized vision-language connectors or leveraging visual instruction tuning from diverse domains. In this paper, we tackle this issue from a fundamental yet unexplored perspective by revisiting the core architecture of MLLMs. Most MLLMs are typically built on decoder-only LLMs consisting of a causal attention mechanism, which *limits the ability of earlier modalities (e.g., images) to incorporate information from later modalities (e.g., text)*. To address this problem, we propose  AKI, a novel MLLM that unlocks causal attention into modality-mutual attention (MMA) to enable image tokens to attend to text tokens. This simple yet effective design allows AKI to achieve superior performance in 12 multimodal understanding benchmarks (+7.2% on average) without introducing additional parameters and increasing training time. Our MMA design is intended to be generic, allowing for application across various modalities, and scalable to accommodate diverse multimodal scenarios. The code is publicly available at <https://github.com/sony/aki>, and we will release our AKI-4B model to encourage further advancements in MLLMs across various directions.

1 Introduction

Recently, Multimodal Large Language Models (MLLMs) have demonstrated remarkable capabilities in multimodal understanding [3, 33, 26, 44, 21], paving the way for innovative applications in general-purpose foundation models [46]. By leveraging visual instruction tuning [27] with large-scale vision-text datasets spanning diverse domains (e.g., Visual Question Answering (VQA), Optical Character Recognition (OCR), and coding), MLLMs can generate coherent and contextually accurate responses to user queries involving both visual and textual inputs [1, 41]. Despite these advancements, a significant concern limiting the reliability and applicability of MLLMs is the issue of object hallucinations, where the generated outputs are not factually aligned with the provided inputs [28]. This limitation becomes especially evident in tasks demanding robust cross-modal interactions, such as vision-centric tasks (e.g., object counting, spatial relations) requiring accurate object-location descriptions. Figure 1 illustrates a vision-centric paradigm that has ambiguous signs in the image. Both the proprietary model (GPT-4o [35]) and open-source models (Molmo [10], and DeepSeek-VL2-Small [41]) suffer from object hallucinations by responding to the user query with inaccurate *No Parking* and *Passenger Loading* signs.

*Corresponding Author.

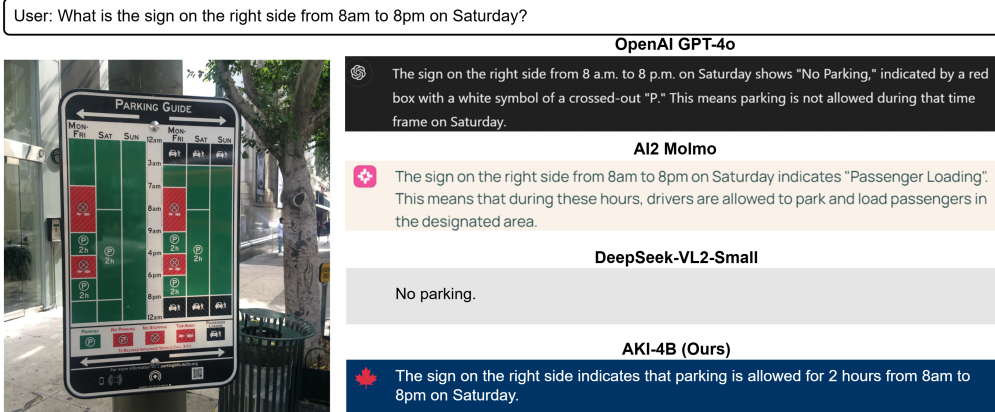


Figure 1: An illustration of the vision-centric scenario. The image contains ambiguous signs with the object-related query. The correct answer is that parking is allowed for 2 hours from 8am to 8pm on Saturday. While GPT-4o [35], Molmo [10], and DeepSeek-VL2-Small [41] respond with hallucinations, our proposed AKI is able to provide accurate answer. The image is sourced from [36].

Previous research has mitigated the vision-language misalignment issue through various approaches. One promising direction involves data-centric approaches, which scale up the diversity of vision-related instruction data during the supervised finetuning stage. For instance, Molmo [10] incorporates not only conventional academic datasets but also specialized datasets, such as clocks, pointing, and counting tasks, to ground visual understanding. Similarly, LLaVA-1.5 [26] and the MM-1 as well as MM-1.5 series [33, 52] also demonstrate the effectiveness of multimodal understanding by expanding the range of visual instruction samples. Another key direction focuses on vision-language connectors, which aim to improve the alignment between visual and textual representations. Cha et al. [9] introduced abstractors that provide both flexibility and locality preservation, while Tong et al. [38] proposed spatial vision aggregators that explicitly define the aggregation space for each query token and repeatedly aggregate vision features across LLM layers. Nonetheless, the challenge of scaling training data remains a significant barrier for researchers with limited resources. Furthermore, design choices for vision-language connectors have yet to reach a consensus on their optimal implementation [33].

In this paper, we tackle the misalignment issue from a fundamental yet unexplored perspective by revisiting the major component of MLLMs. As illustrated in Figure 2, most existing MLLMs are built on top of LLMs that incorporate the causal attention mechanism, which was originally designed to prevent earlier text tokens from attending to future text tokens in autoregressive text generation. Taking a single image-text pair as an example, to accommodate multimodal input for the LLM, the input sequence is typically formed by placing image tokens before text tokens. However, this design introduces a critical limitation: the former modality (images) cannot attend to or incorporate information from the latter modality (text), thereby hindering effective cross-modal interactions. This limitation raises a fundamental question: *How can we enable the former modality to effectively consider and integrate information from the latter modality in MLLMs?*

An intuitive solution to this problem involves directly pretraining and finetuning an MLLM using both image-text and text-image input orders, which can be easily implemented within existing training pipelines and enhances robustness by exposing the model to different input sequences. While this method shows improvements on some multimodal understanding benchmarks (see our experiments in Section 4.2 for details), it doubles the required training time for each stage and incurs exponential growth in training costs as the number of modalities increases. To address this, we propose AKI, a novel MLLM that redefines the causal attention mechanism into modality-mutual attention (MMA) within the LLM. Specifically, attention masks in the LLM are modified to allow image tokens to attend to the question text tokens during the supervised finetuning stage. This *unlock* strategy offers multiple key advantages: 1) image tokens gain the ability to access and interpret user queries; 2) it solely modifies the attention masks within the LLM, enabling seamless integration into existing MLLM training frameworks; and 3) no additional parameters or training time are introduced.

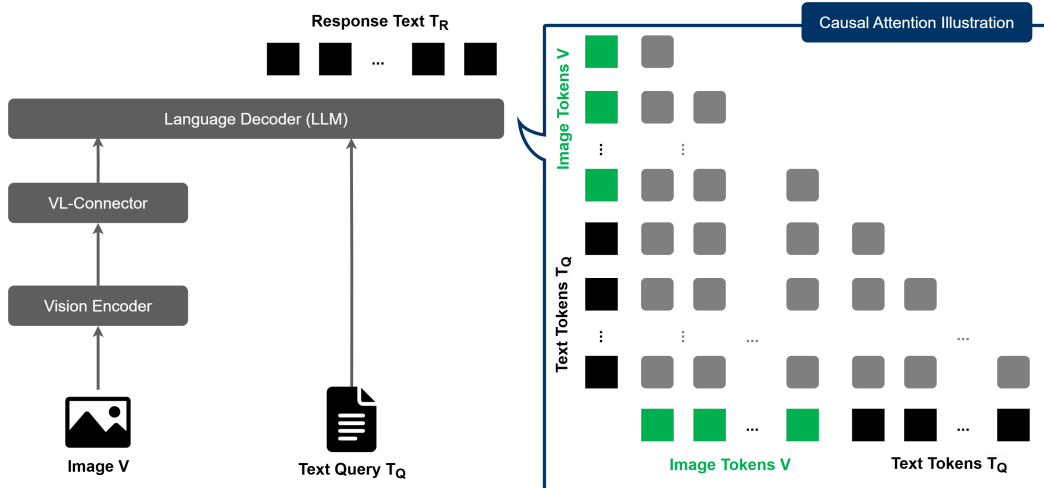


Figure 2: The conventional framework for MLLMs (e.g., Molmo [10], BLIP-3 [44], and Cambrian [38]) typically consists of a vision encoder, a vision-language (VL) connector, and a text decoder (LLM). In this framework, images are often placed before text in a sequentialized input, causing the former modality (images) lacking access to information from the later modality (text) due to the causal attention design in decoder-only LLMs, as shown in the right part (gray squares). Notably, placing text before image tokens does not resolve this issue, as the fundamental limitation persists.

Compared to the conventional causal-attention framework, state-of-the-art baselines, and our intuitive dual-order method, all using the same training data and configurations, our simple yet effective MMA approach consistently demonstrates significant improvements across 12 multimodal benchmarks (+7.2% average performance gain compared to the state-of-the-art baseline [43]), including vision-centric, knowledge-based, and general tasks. Finally, we scale up our model with a larger number of training data, achieving superior performance compared to both open-source and proprietary models of similar size across most benchmarks.

In particular, our contributions are summarized as three-fold:

- We address the vision-language misalignment issue by revisiting the foundational framework of MLLMs and identifying a critical limitation in the causal attention mechanism of LLMs when processing multimodal inputs. Specifically, we highlight that the sequential input design prevents the earlier modality from accessing information from the latter modality.
- To overcome this limitation, we first explore an intuitive approach that demonstrates the importance of enabling cross-modal information flow, though it incurs additional training costs. Therefore, we propose **AKI**, an MLLM equipped with modality-mutual attention to mitigate object hallucinations by cross-modal understanding. By unlocking the attention masks to allow tokens from the former modality to attend to contextual information from the latter modality, our approach provides a generic and scalable solution that is expected to extend seamlessly to other – and potentially multiple – modalities.
- Through extensive evaluations on 12 multimodal understanding benchmarks, our MMA approach consistently outperforms state-of-the-art models and carefully designed variant baselines, demonstrating its effectiveness in advancing multimodal reasoning and understanding.

2 Related Works

2.1 Multimodal Large Language Models

In recent years, the rapid development of MLLMs has been witnessed with their capabilities to comprehend and process multimodal information, reinforcing them to perceive, reason, and respond

across diverse applications [46]. Building on earlier milestones, such as Flamingo [2], which pioneered the integration of visual and textual information, recent advancements (e.g., LLaVA-1.5 [26], QWen-VL [7], GPT-4o [35], Phi-3-Vision [1], and Claude 3.5-Sonnet [4]) have employed visual instruction tuning [27] to imbue models with domain-specific expertise, enhancing their ability to ground visual information effectively. Generally, as illustrated in Figure 2, most MLLMs share a standard architecture comprising three core components [8]: a vision encoder (often a CLIP-style) to extract image features, a vision-language (VL) connector to align visual embeddings with textual representations, and a text decoder (LLM) to reason over the combined image-text inputs and serve as the user-facing inference interface. Despite these substantial advancements, the misalignment issue between visual contents and textual responses remains an emerging challenge, which often results in inaccurate or inconsistent outputs by heavily depending on the knowledge of LLMs, posing a significant hurdle especially to the vision-centric applications [38].

2.2 Vision-Language Misalignment

Existing works addressing the misalignment issue with end-to-end manners can be mainly categorized into two strategies. The first category comprises data-centric approaches, which focus on collecting diverse visual instruction tuning samples by annotating images with vision models or human input, followed by generating question-answer pairs using LLMs [47, 53, 11, 10]. Although these methods enhance the fine-grained grounding capabilities of MLLMs, scaling data for training MLLMs remains a costly endeavor, especially for researchers with limited computational resources. The other alternative involves model-centric methods, which mainly aim to improve the vision-language connector, an important component for aligning vision and text representations. Common approaches include resamplers [2], Q-Formers [22], and linear projectors [27], all of which are widely adopted in many MLLMs. Recently, locality-preserved abstractors [9] have demonstrated superior performance compared with earlier connectors; similarly, Cambrian [38] introduced a spatial vision aggregator by explicitly defining the aggregation space and incorporating vision features across LLM layers. However, as empirically experimented in [33], no single vision-language connector consistently outperforms across diverse multimodal benchmarks, leaving their optimal design an open question.

From a more foundational perspective, we explore the misalignment issue by revisiting the core architecture of LLMs, where causal attention prevents the earlier modality (e.g., images) from attending to the later modality (e.g., text). The concept of concentric causal attention (CCA) [43] is closely related to our work, as it manipulates position encoding and attention masks for image tokens to prevent hallucinations; nonetheless, CCA assumes central regions of an image are more critical, and still suffers from the cross-modal interaction issue. Our proposed modality-mutual attention, on the flip side, unlocks causal attention between modalities for cross-modal interactions, achieving effective alignment performance across extensive multimodal benchmarks.

3 How to Enable the Former Modality to See the Latter Modality?

3.1 Overview

Generally, we follow the standard pipeline illustrated in Figure 2, which first divides an image into multiple patches that are fed into the vision encoder f_V to produce vision representations. Then, the LLM f_L integrates these representations, which are first processed by the vision-language connector p_V , with text representations encoded from the text query – e.g., captions in the pretraining (PT) stage, question-answer pairs in the supervised finetuning (SFT) stage – to generate a response autoregressively. Formally, given an image-text pair $S = [V, T_Q]^2$, where the image V appears first, followed by the text query T_Q , with the corresponding length $|V|$ and $|T_Q|$, respectively, the objective is to generate a response T_R as:

$$T_R = f_L(H_V, H_{T_Q}), \text{ where } H_V = f_V(p_V(V)) \in \mathbb{R}^{|V| \times d}; H_{T_Q} = f_T(T_Q) \in \mathbb{R}^{|T_Q| \times d}, \quad (1)$$

where f_T is the text token embedder in the LLM and d is the hidden dimension of the LLM.

To enforce autoregressive generation, where tokens are only allowed to have access to their corresponding previous tokens, LLMs are built using decoder-only Transformers with causal attention and

²In the SFT stage, a system message is placed before V similar to [9]. We omit the system text tokens in this section for better readability.

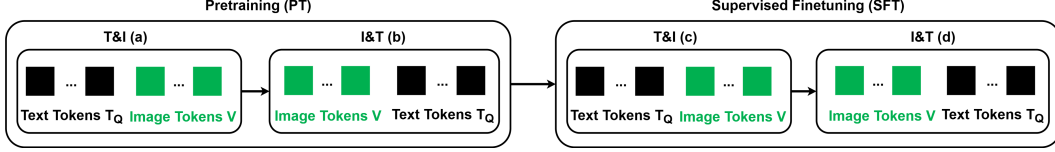


Figure 3: An illustration for dual-order training, where T and I indicate text and images, respectively.

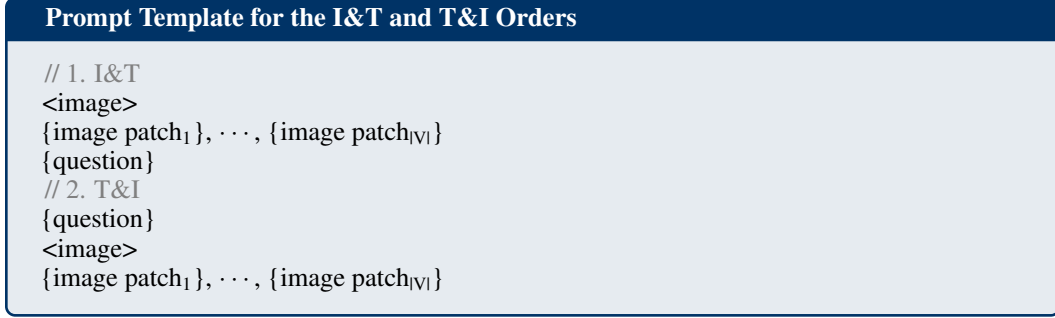


Figure 4: The prompt template for the I&T and T&I input orders. {image patch} and {question} are replaced based on each data sample.

feed-forward networks [39]. Specifically, causal attention can be formulated as follows:

$$Attention_{causal} = softmax\left(\frac{QK^T + M}{\sqrt{d}}\right), \text{ where } M_{ij} = \begin{cases} 0 & \text{if } j \leq i, \\ -\infty & \text{if } j > i, \end{cases} \quad (2)$$

where M is the triangular indicator matrix ensuring that only positions $j \leq i$ are attended to by applying $-\infty$ to disallowed positions.

3.2 Intuitive Approach: Dual-Order Training (DOT)

The conventional pipeline for training an MLLM follows the I&T order in both the PT and SFT stages (i.e., only (b) and (d) in Figure 3), where image tokens precede text tokens in the sequence $S = [V, T_Q]$. To mitigate modality blindness, we introduce a dual-order training (DOT) method that further trains the model using the T&I order, $\hat{S} = [T_Q, V]$. As illustrated in Figure 3, we opt for a tandem training pipeline, where the model is first trained with the T&I order, followed by the I&T order in each stage, ensuring alignment with the I&T order during inference:

$$\text{Conventional: } [V_{PT}, T_{Q_{PT}}] \rightarrow [V_{SFT}, T_{Q_{SFT}}]. \quad (3)$$

$$\text{DOT: } [T_{Q_{PT}}, V_{PT}] \rightarrow [V_{PT}, T_{Q_{PT}}] \rightarrow [T_{Q_{SFT}}, V_{SFT}] \rightarrow [V_{SFT}, T_{Q_{SFT}}]. \quad (4)$$

This strategy learns robust representations by incorporating not only the standard I&T but also T&I orders during training. In addition, it provides a plug-and-play advantage, as it merely requires reordering text and image inputs before feeding them into the model. Nonetheless, compared with the conventional pipeline (Equ. 3), a key drawback is the increased computational cost as shown in Equ. 4 due to the need for training both orders, requiring twice the training time per stage. Note that this overhead scales factorially to $n!$ when the input consists of n modalities. The prompt template for incorporating I&T and T&I orders is described in Figure 4.

3.3 🍁AKI: MLLMs with Modality-Mutual Attention (MMA)

When incorporating multimodal inputs, most open-source and proprietary MLLMs (e.g., MM-1.5 [52], LLaVa-1.5 [26]) follow earlier approaches (e.g., Flamingo [2]) by positioning images before text in the input sequence. While this I&T order allows text to reference visual information, it blocks the path for images to see textual information due to causal attention in the LLM, which may be one of the reasons why MLLMs are prone to vision-centric tasks [38]. For instance, when describing the

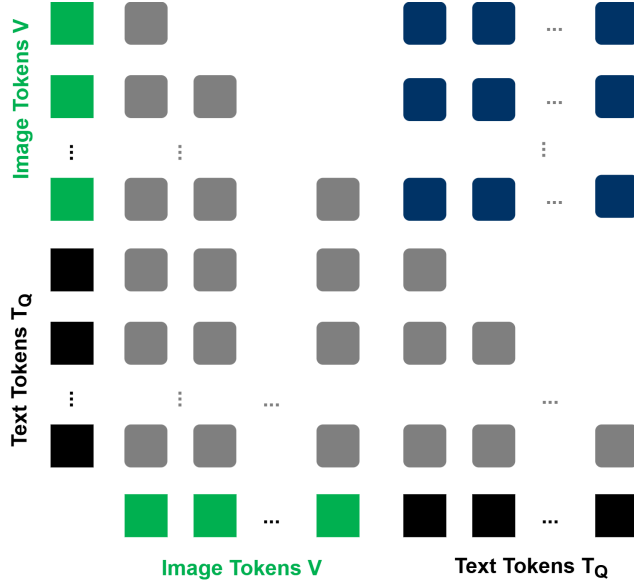


Figure 5: An illustration for our proposed modality-mutual attention (MMA), which modifies the causal attention mask in the LLM (gray squares) by enabling the information flow from image tokens to text tokens (blue squares).

object count as a user query, the model would need the text input (perhaps including object names or relations) to inform its understanding of the image. Moreover, simply reversing the modality order (i.e., T&I) does not resolve the issue, as text tokens still cannot attend to image tokens. Therefore, causal attention, which is designed to prevent information leakage in unimodal settings, is inadequate for MLLMs, where effective multimodal interactions are essential.

To this end, we propose modality-mutual attention that alters the causal attention mechanism in the LLM. As illustrated in Figure 5, our approach replaces the standard causal attention mask by unlocking the paths that allow image tokens to attend to text tokens, all without requiring the LLM retraining from scratch. Formally, M in Equ. 2 can be devised as M' :

$$M'_{ij} = \begin{cases} 0 & \text{if } j \leq i, \\ 0 & \text{if } 1 \leq i \leq |V| \text{ and } |V| + 1 \leq j \leq |V| + |T_Q|, \\ -\infty & \text{otherwise.} \end{cases} \quad (5)$$

In this manner, the image tokens are able to see text tokens, making our approach a generalizable solution for any multimodal model leveraging causal attention in generation. Furthermore, while we focus on single image-text pairs in this paper, our approach naturally extends to interleaved multimodal data, where greater cross-modal visibility is essential for capturing rich multimodal interactions. To accommodate such cases, we propose a generalized condition:

$$M'_{ij} = \begin{cases} 0 & \text{if } j \leq i \text{ or } \phi(i) \neq \phi(j), \\ -\infty & \text{if otherwise,} \end{cases} \quad (6)$$

where $\phi(i)$ maps i -th token to its corresponding modality (e.g., audio, image, text).

The modality-mutual attention is only applied with the given input S to be stored in the KV cache – the generated tokens (i.e., T_R) employ the standard causal attention as in Equ. 2. In this paper, we focus on applying our modality-mutual attention during the SFT stage since the pretraining stage aims at understanding the context of the image-text pairs; there is no specific user instruction or questions that can specify image tokens to attend to (e.g., “How many cars are in the image?”).

3.4 Training

To ensure fair comparisons, we train both the DOT and MMA methods using a standard two-stage pipeline, consisting of pretraining and supervised finetuning. During both stages, we freeze the vision

encoder and unfreeze the VL-connector and LLM to enhance the model’s capability in vision-text alignment and multimodal understanding. We train the LLM with all parameters instead of parameter-efficient finetuning. To learn vision-text alignment, Blip3-kale [6] is adopted as the pretraining captioning dataset to understand how visual signals align with textual captions. To equip our AKI model (Section 4.3) with OCR capabilities, we further train it on 5M OCR samples using Blip3-ocr-200m [44] with basic text extraction. Following pretraining, the supervised finetuning stage aims to equip the model with instruction-following abilities while further improving its capacity for diverse multimodal comprehension.

Similar to [9], we incorporate a range of datasets to cover different multimodal reasoning tasks: 1) VQAv2 [16], VSR [25], GQA [17], and OCRVQA [34] for learning open-ended VQA; 2) ScienceQA [31] and A-OKVQA [37] for learning multi-choice VQA; 3) RefCOCO [18], RefCOCOg [32], RefCOCO+ [48], and VisualGnome [19] for referring expression comprehension (visual grounding and grounded captioning); and 4) Llava-150k [27] for visual instruction-following. Detailed statistics, dataset descriptions, and templates including instructions are depicted in Appendix A.2 and B.

4 Experiments

4.1 Experimental Setup

Benchmarks. We evaluate AKI on a diverse collection of 12 multimodal understanding benchmarks, which can be categorized into 3 groups to assess multifacet capabilities.

1) General: MME [14] assesses perception and cognitive abilities across multiple subtasks. We denote its perception and cognition splits as MME^P and MME^C , respectively. MMBench (MMB) [29] evaluates answer robustness by applying extensive shuffling to multiple-choice answers. SEED-Bench [20] is a multi-choice VQA task covering multifaceted understanding. We evaluate its image-based subset, denoted as SEED^I. LLaVA-Bench (LLaVA^W) [27] assesses the correctness and helpfulness of visual conversations across diverse tasks using LLM-as-a-judge.

2) Knowledge: MMMU [50] measures college-level perception and reasoning with domain-specific knowledge. MathVista [30] evaluates mathematical reasoning in visual contexts. We use the test-mini set, denoted as MathV^{mini}.

3) Vision-Centric: POPE [23] measures object hallucination in multimodal models. MM-Vet [49] examines MLLMs with multidisciplinary, complex questions and employs LLMs to evaluate the quality of open-ended responses. RealworldQA [42] focuses on vision-centric tasks, evaluating spatial understanding from real-world images. CV-Bench [38] assesses vision-centric capabilities, including 2D spatial relationships and object counting (CV-Bench^{2D}) as well as 3D depth ordering and relative distance (CV-Bench^{3D}).

Evaluation metrics. The evaluation metrics for each benchmark are computed using official implementations by default, and all experiments are conducted in a 0-shot manner. Except for CV-Bench, we leverage the VLMEval toolkit [12] to fairly evaluate the performance of the baselines and our AKI model. In terms of CV-Bench, we report 2D and 3D accuracy separately following the official evaluation codes.

Implementation details. All experiments in Section 4.2 and AKI-4B are adopted Phi-3.5-mini-instruct [1] as the pretrained LLM, the Perceiver Resampler [2] as the VL connector to map visual representations into the textual space, and SigLIP [51] as the vision encoder, following empirical validation in [38]. We focus on relatively smaller scale (i.e., AKI-4B) compared to existing advancements on large-scale models, which has gained attention due to its cost-effectiveness for deployment on edge devices since the objective of this paper is to demonstrate improvements driven by fundamental model modifications. Following [44], we set the resolution of pretraining images to 384×384 pixels to align with SigLIP. The number of vision tokens is fixed at 144. The global batch sizes for pretraining and finetuning are 192 and 64, respectively. To analyze the impact of modality-mutual attention, we adopt a short training schedule for rapid iteration across all models in Section 4.2. Specifically, we set the number of pretraining and finetuning steps to 50k and 5k, respectively. For our final model (Section 4.3), the numbers of pretraining and finetuning steps are enlarged to 275k (250k for Blip3-kale and 25k for Blip3-ocr-200m) and 10k, respectively. More details are provided in Appendix A.

	General					Knowledge		Vision-Centric				
	MME ^P	MME ^C	MMB	SEED ^J	LLaVA ^w	MMMU	MathV ^{mini}	POPE	MM-Vet	RealWorldQA	CV-Bench ^{2D}	CV-Bench ^{3D}
(I&T) _{PT} + (I&T) _{SFT}	1226.3	258.2	64.9	64.1	47.0	31.1	24.2	79.8	24.3	50.6	45.2	54.3
CCA [43]	<u>1212.7</u>	<u>243.6</u>	<u>67.4</u>	<u>65.3</u>	<u>54.0</u>	<u>34.6</u>	<u>25.6</u>	<u>81.9</u>	<u>29.0</u>	52.7	<u>56.0</u>	62.8
(w/o T&I) _{PT}	1046.3	226.4	31.7	45.1	38.1	27.2	23.8	65.0	17.2	40.1	53.2	54.8
(w/o I&T) _{PT}	1013.2	208.6	32.0	43.3	37.9	27.7	22.4	70.4	20.6	39.5	55.4	53.0
(w/o T&I) _{SFT}	1194.8	<u>289.3</u>	58.5	61.1	40.2	28.0	21.9	79.0	22.8	47.8	41.4	<u>63.0</u>
(w/o I&T) _{SFT}	1166.2	264.3	58.4	60.8	36.9	26.7	23.1	76.8	20.4	46.9	43.3	61.2
DOT (Ours)	<u>1267.8</u>	251.4	43.8	54.7	47.5	30.7	<u>25.6</u>	82.7	25.0	50.5	52.2	58.1
MMA (Ours)	1363.7	315.4	71.8	67.1	59.6	37.3	26.4	82.7	30.2	<u>52.3</u>	57.8	64.1
Improvements	10.9%	29.5%	4.3%	2.8%	10.4%	7.8%	3.1%	1%	4.1%	-	3.2%	2.1%

Table 1: Apples-to-apples comparisons between the commonly-used (I&T)_{PT} + (I&T)_{SFT} pipeline (e.g., Molmo [10], BLIP-3 [44], and Cambrian [38]), CCA [43], variants of dual-order training (DOT), and our modality-mutual attention (MMA) under the same training configurations and datasets. Note that CCA and MMA also follow the (I&T)_{PT} + (I&T)_{SFT} training pipeline. Performance improvements are calculated relative to the state-of-the-art CCA approach. The best performance in each column is in **boldface** while the second-best result is underlined. Benchmark names are abbreviated due to space limits. The detailed metrics are reported in Appendix C.2.

4.2 Impacts on Modality-Mutual Attention

To evaluate the effectiveness of the proposed modality-mutual attention (MMA), we conduct a comprehensive comparison against several approaches under identical training configurations, pre-training, and supervised finetuning datasets to ensure fair, apples-to-apples comparisons: **1) (I&T)_{PT} + (I&T)_{SFT}** refers to the widely used training pipeline (e.g., Molmo [10], BLIP-3 [44], and Cambrian [38]), where image tokens are placed before text tokens in both the pretraining and finetuning stages (i.e., steps (b) and (d) in Figure 3). **2) Concentric Causal Attention (CCA)** [43] modifies the positions and attention masks of image tokens and represents the state-of-the-art method for mitigating object hallucinations without introducing additional parameters or datasets. Additionally, **3) the dual-order training (DOT) method** is included along with three variants to examine the impact of cross-modal interactions on multimodal performance: 3.1) without T&I order in the PT stage (w/o T&I)_{PT}, 3.2) without I&T order in the PT stage (w/o I&T)_{PT}, 3.3) without T&I order in the SFT stage (w/o T&I)_{SFT}, 3.4) without I&T order in the SFT stage (w/o I&T)_{SFT}.

Table 1 summarizes the overall performance across these methods, demonstrating that our MMA approach consistently outperforms all baselines and variants on 11 out of 12 benchmarks. Quantitatively, MMA achieves performance improvements ranging from 1% to 30% compared to CCA, and the qualitative comparisons are illustrated in Appendix D. Key observations from our findings are highlighted as follows:

The effects of dual-order training. The comparison between (I&T)_{PT} + (I&T)_{SFT} and DOT highlights the importance of considering cross-modal interactions, showing that training the model on the same dataset but incorporating an additional text-then-image order in both the PT and SFT stages improves vision-centric performance (e.g., POPE, MM-Vet, and CV-Bench). This signifies that explicitly enabling modalities to interact to each other enhances vision-centric capabilities, particularly for tasks where images need to be interpreted in relation to object-related text queries. Although removing any order during training generally results in inferior performance compared to DOT, some configurations still yield better results. This detrimental effect indicates that simply introducing cross-modal interactions with different orders may confuse the model, likely due to the varying positions of images across samples. Furthermore, adding the T&I order in the SFT stage ((w/o T&I)_{PT}) is more prone to negative impacts than introducing it in the PT stage ((w/o T&I)_{SFT}), which demonstrates that the PT stage with diverse input orders is able to help the model learn more robust multimodal representations.


	General					Knowledge		Vision-Centric				
	MME ^P	MME ^C	MMB ^{dev}	SEED ^J	LLaVA ^w	MMMU	MathV ^{mini}	POPE	MM-Vet	RealWorldQA	CV-Bench ^{2D}	CV-Bench ^{3D}
3B Model Comparisons												
<i>Proprietary</i>												
MM1-3B [†] [33]	1482.5	279.3	67.8	68.8	72.1	33.9	32.0	87.4	43.7	-	-	-
MM1.5-3B [†] [52]	1478.4	319.6	-	72.4	73.0	37.1	44.4	88.1	41.0	56.9	-	-
<i>Open-source</i>												
DeepSeek-VL-1.3B	1306.6	225.0	-	66.0	51.1	33.8	30.7	85.9	29.2	49.7	-	-
MiniCPM-V2-3B [45]	1411.4	396.8	69.1	67.1	69.2	38.2	39.8	86.3	41.0	55.8	-	-
VILA-1.5-3B [24]	1379.3	268.2	62.4*	68.0	65.5	34.2	31.8	86.8	38.8	53.2	50.1*	60.3*
Phi-3-Vision-4B [1]	1205.1	302.9	74.2*	70.9	63.9	46.1	44.8	83.7	44.1	58.8	60.7*	68.2*
BLIP-3-4B [44]	1487.6	302.9	76.0*	71.8	69.8	40.1	40.1	86.9	41.0	61.6	66.2*	75.4*
Qwen2-VL-2B [40]	1485.1	413.9	-	72.4	50.5	42.2	48.0	87.3	51.5	60.7	-	-
 AKI-4B (Ours)	1491.9	362.9	73.1	69.4	74.6	38.7	32.1	86.9	40.8	58.9	62.1	71.8
7B Model Comparisons												
LLaVA-1.5-7B [26]	1506.2	302.1	64.3 [†]	65.8	61.8	35.7	25.5	86.1	32.9	54.8	-	-
Honeybee-C-7B [†] [9]	1584.2	307.1	70.1	64.5	67.1	35.3	-	83.2	34.9	-	-	-

Table 2: Comparisons with state-of-the-art models. Results are from the OpenVLM leaderboard, the results with * are from [44], and the results with [†] refer to the corresponding official papers. The best performance within the 3B group is in **boldface**. The detailed metrics for each benchmark of AKI-4B are reported in Appendix C.2.

The performance of MMA. Since DOT remains deficient for overall multimodal understanding while doubling the training time, our modality-mutual attention (MMA) consistently outperforms all approaches across nearly all benchmarks. In general, CCA, despite not introducing additional parameters or increasing training time, surpasses both the (I&T)_{PT} + (I&T)_{SFT} and DOT, highlighting the inefficiencies of the conventional vision-language framework. Meanwhile, our proposed MMA significantly and consistently outperforms CCA across various benchmarks, which is attributed to its unlocked design that enables effective cross-modal attention within the LLM. Notably, compared to the (I&T)_{PT} + (I&T)_{SFT}, MMA improves not only vision-centric tasks but also general VQA tasks. In contrast, CCA’s focus on central image positions negatively impacts performance on the MME benchmark, leading to a greater performance decline compared to MMA on the general benchmarks.


4.3 Comparisons with State-of-the-Art MLLMs

To push the limits of MLLMs with the MMA design, we evaluate our AKI-4B model, trained on an extended schedule, against state-of-the-art MLLMs, as shown in Table 2. Moreover, OCR data is incorporated to enhance the model’s ability to understand text within images. Our results show that AKI-4B outperforms 7B-scale MLLMs with comparable training data across all benchmarks except for MME_P, highlighting the potential of integrating MMA into the conventional MLLM pipeline.

Despite being trained on significantly smaller datasets (e.g., 6.7B pretraining tokens in AKI-4B vs. 1.4T pretraining tokens in QWen2-VL), with lower image resolutions (e.g., 384x384 in AKI-4B vs. 2016x2016 in MM-1.5 as well as 1344x1344 in MiniCPM-V2) and fewer vision tokens (e.g., 144 in AKI-4B vs. 640 in MiniCPM-V2), AKI-4B demonstrates highly remarkable performance in terms of general as well as vision-centric tasks, even achieving the best results for MME_P and LLaVA_w. Since we incorporate only a small amount of knowledge-based fine-tuning data, AKI-4B is expected to be inferior to existing MLLMs in the knowledge domain. Although our AKI-4B model does not support interleaved inputs, it still performs on par with other MLLMs on the MMMU benchmark, which includes some interleaved samples. For such cases, we use only the first image for inference.

These findings suggest that existing MLLMs could further expand the boundaries of multimodal understanding by integrating our proposed MMA design.

5 Conclusions

This paper proposes AKI, a multimodal LLM with the novel modality-mutual attention design, to tackle vision-language misalignment from a fundamental architecture perspective. Distinct from existing MLLMs in which image tokens fail to consider the information from the text tokens due to the causal attention design in the LLM, our modality-mutual attention enables tokens from the earlier modality to be able to attend to tokens from the latter modality by unlocking attention masks for cross-modal interactions. Our proposed MMA significantly outperforms the baseline with causal attention, intuitive dual-order training methods, and the state-of-the-art approach on 12 extensive multimodal understanding benchmarks without introducing extra parameters and training costs. When scaling up with comparable amounts of pretraining samples, our AKI-4B model is superior to existing MLLMs on various benchmarks. We believe modality-mutual attention serves as a generic and scalable design for other multi-modalities.

6 Broader Impacts and Limitation

6.1 Broader Impacts

As our modality-mutual attention operates on the attention mask in the LLM, it benefits not only vision-language generative pretraining (e.g., [13]) but also generalizes to X-language modalities, where X represents other modalities (e.g., audio). Moreover, this design can be incorporated into other multimodal data (e.g., image-audio) that involve causal attention in generation. It is also expected to be scalable for hierarchical inputs, such as tabular structures and text-image interleaved data. By open-sourcing our code and models without introducing additional parameters, we aim to provide researchers with the tools to tackle real-world multimodal challenges and drive advancements in MLLMs from a fundamental perspective.

6.2 Limitation

Despite its effective multimodal understanding capabilities, the major limitation of AKI is that the proposed modality-mutual attention only provides benefits during the SFT stage. Applying it directly in the PT stage leads to information leakage – earlier text tokens can access future text tokens through the attention path to image tokens, which, in turn, can attend to future text tokens. This issue arises because the PT stage relies solely on captioning samples, which lack specific questions or inquiries as seen in the SFT stage that could explicitly restrict image tokens’ attentions. We leave this for future work, as we believe that addressing multimodal misalignment from a fundamental design perspective remains an unexplored yet critical challenge.

References

- [1] Abdin, M.I., Jacobs, S.A., Awan, A.A., Aneja, J., Awadallah, A., Awadalla, H., Bach, N., Bahree, A., Bakhtiari, A., Behl, H.S., Benhaim, A., Bilenko, M., Bjorck, J., Bubeck, S., Cai, M., Mendes, C.C.T., Chen, W., Chaudhary, V., Chopra, P., Giorno, A.D., de Rosa, G., Dixon, M., Eldan, R., Iyer, D., Garg, A., Goswami, A., Gunasekar, S., Haider, E., Hao, J., Hewett, R.J., Huynh, J., Javaheripi, M., Jin, X., Kauffmann, P., Karampatziakis, N., Kim, D., Khademi, M., Kurilenko, L., Lee, J.R., Lee, Y.T., Li, Y., Liang, C., Liu, W., Lin, E., Lin, Z., Madan, P., Mitra, A., Modi, H., Nguyen, A., Norick, B., Patra, B., Perez-Becker, D., Portet, T., Pryzant, R., Qin, H., Radmilac, M., Rosset, C., Roy, S., Ruwase, O., Saarikivi, O., Saied, A., Salim, A., Santacrose, M., Shah, S., Shang, N., Sharma, H., Song, X., Tanaka, M., Wang, X., Ward, R., Wang, G., Witte, P., Wyatt, M., Xu, C., Xu, J., Yadav, S., Yang, F., Yang, Z., Yu, D., Zhang, C., Zhang, C., Zhang, J., Zhang, L.L., Zhang, Y., Zhang, Y., Zhang, Y., Zhou, X., 2024. Phi-3 technical report: A highly capable language model locally on your phone. CoRR abs/2404.14219.

- [2] Alayrac, J., Donahue, J., Luc, P., Miech, A., Barr, I., Hasson, Y., Lenc, K., Mensch, A., Millican, K., Reynolds, M., Ring, R., Rutherford, E., Cabi, S., Han, T., Gong, Z., Samangooei, S., Monteiro, M., Menick, J.L., Borgeaud, S., Brock, A., Nematzadeh, A., Sharifzadeh, S., Binkowski, M., Barreira, R., Vinyals, O., Zisserman, A., Simonyan, K., 2022. Flamingo: a visual language model for few-shot learning, in: *NeurIPS*.
- [3] Anil, R., Borgeaud, S., Wu, Y., Alayrac, J., Yu, J., Soricut, R., Schalkwyk, J., Dai, A.M., Hauth, A., Millican, K., Silver, D., Petrov, S., Johnson, M., Antonoglou, I., Schrittwieser, J., Glaese, A., Chen, J., Pitler, E., Lillicrap, T.P., Lazaridou, A., Firat, O., Molloy, J., Isard, M., Barham, P.R., Hennigan, T., Lee, B., Viola, F., Reynolds, M., Xu, Y., Doherty, R., Collins, E., Meyer, C., Rutherford, E., Moreira, E., Ayoub, K., Goel, M., Tucker, G., Piqueras, E., Krikun, M., Barr, I., Savinov, N., Danihelka, I., Roelofs, B., White, A., Andreassen, A., von Glehn, T., Yagati, L., Kazemi, M., Gonzalez, L., Khalman, M., Sygnowski, J., et al., 2023. Gemini: A family of highly capable multimodal models. *CoRR abs/2312.11805*.
- [4] Anthropic, 2024. Claude 3.5 sonnet. <https://www.anthropic.com/news/claude-3-5-sonnet>.
- [5] Awadalla, A., Gao, I., Gardner, J., Hessel, J., Hanafy, Y., Zhu, W., Marathe, K., Bitton, Y., Gadre, S.Y., Sagawa, S., Jitsev, J., Kornblith, S., Koh, P.W., Ilharco, G., Wortsman, M., Schmidt, L., 2023. Openflamingo: An open-source framework for training large autoregressive vision-language models. *CoRR abs/2308.01390*.
- [6] Awadalla, A., Xue, L., Shu, M., Yan, A., Wang, J., Purushwalkam, S., Shen, S., Lee, H., Lo, O., Park, J.S., Guha, E., Savarese, S., Schmidt, L., Choi, Y., Xiong, C., Xu, R., 2024. BLIP3-KALE: knowledge augmented large-scale dense captions. *CoRR abs/2411.07461*.
- [7] Bai, J., Bai, S., Yang, S., Wang, S., Tan, S., Wang, P., Lin, J., Zhou, C., Zhou, J., 2023. Qwen-vl: A frontier large vision-language model with versatile abilities. *CoRR abs/2308.12966*.
- [8] Caffagni, D., Cocchi, F., Barsellotti, L., Moratelli, N., Sarto, S., Baraldi, L., Cornia, M., Cucchiara, R., 2024. The revolution of multimodal large language models: A survey, in: *ACL (Findings)*, Association for Computational Linguistics. pp. 13590–13618.
- [9] Cha, J., Kang, W., Mun, J., Roh, B., 2024. Honeybee: Locality-enhanced projector for multimodal LLM, in: *CVPR*, IEEE. pp. 13817–13827.
- [10] Deitke, M., Clark, C., Lee, S., Tripathi, R., Yang, Y., Park, J.S., Salehi, M., Muennighoff, N., Lo, K., Soldaini, L., Lu, J., Anderson, T., Branson, E., Ehsani, K., Ngo, H., Chen, Y., Patel, A., Yatskar, M., Callison-Burch, C., Head, A., Hendrix, R., Bastani, F., VanderBilt, E., Lambert, N., Chou, Y., Chheda, A., Sparks, J., Skjongsberg, S., Schmitz, M., Sarnat, A., Bischoff, B., Walsh, P., Newell, C., Wolters, P., Gupta, T., Zeng, K., Borchardt, J., Groeneveld, D., Dumas, J., Nam, C., Lebrecht, S., Wittlif, C., Schoenick, C., Michel, O., Krishna, R., Weihs, L., Smith, N.A., Hajishirzi, H., Girshick, R.B., Farhadi, A., Kembhavi, A., 2024. Molmo and pixmo: Open weights and open data for state-of-the-art multimodal models. *CoRR abs/2409.17146*.
- [11] Dong, H., Kang, Z., Yin, W., Liang, X., Feng, C., Ran, J., 2025. Scalable vision language model training via high quality data curation. *arXiv preprint arXiv:2501.05952*.
- [12] Duan, H., Yang, J., Qiao, Y., Fang, X., Chen, L., Liu, Y., Dong, X., Zang, Y., Zhang, P., Wang, J., et al., 2024. Vlmevalkit: An open-source toolkit for evaluating large multi-modality models, in: *Proceedings of the 32nd ACM International Conference on Multimedia*, pp. 11198–11201.
- [13] Fini, E., Shukor, M., Li, X., Dufter, P., Klein, M., Haldimann, D., Aitharaju, S., da Costa, V.G.T., Béthune, L., Gan, Z., Toshev, A.T., Eichner, M., Nabi, M., Yang, Y., Susskind, J.M., El-Nouby, A., 2024. Multimodal autoregressive pre-training of large vision encoders. *CoRR abs/2411.14402*.
- [14] Fu, C., Chen, P., Shen, Y., Qin, Y., Zhang, M., Lin, X., Qiu, Z., Lin, W., Yang, J., Zheng, X., Li, K., Sun, X., Ji, R., 2023. MME: A comprehensive evaluation benchmark for multimodal large language models. *CoRR abs/2306.13394*.

- [15] Gadre, S.Y., Ilharco, G., Fang, A., Hayase, J., Smyrnis, G., Nguyen, T., Marten, R., Wortsman, M., Ghosh, D., Zhang, J., Orgad, E., Entezari, R., Daras, G., Pratt, S.M., Ramanujan, V., Bitton, Y., Marathe, K., Mussmann, S., Vencu, R., Cherti, M., Krishna, R., Koh, P.W., Saukh, O., Ratner, A.J., Song, S., Hajishirzi, H., Farhadi, A., Beaumont, R., Oh, S., Dimakis, A., Jitsev, J., Carmon, Y., Shankar, V., Schmidt, L., 2023. Datacomp: In search of the next generation of multimodal datasets, in: NeurIPS.
- [16] Goyal, Y., Khot, T., Summers-Stay, D., Batra, D., Parikh, D., 2017. Making the V in VQA matter: Elevating the role of image understanding in visual question answering, in: CVPR, IEEE Computer Society. pp. 6325–6334.
- [17] Hudson, D.A., Manning, C.D., 2019. GQA: A new dataset for real-world visual reasoning and compositional question answering, in: CVPR, Computer Vision Foundation / IEEE. pp. 6700–6709.
- [18] Kazemzadeh, S., Ordonez, V., Matten, M., Berg, T.L., 2014. Referitgame: Referring to objects in photographs of natural scenes, in: EMNLP, ACL. pp. 787–798.
- [19] Krishna, R., Zhu, Y., Groth, O., Johnson, J., Hata, K., Kravitz, J., Chen, S., Kalantidis, Y., Li, L., Shamma, D.A., Bernstein, M.S., Fei-Fei, L., 2017. Visual genome: Connecting language and vision using crowdsourced dense image annotations. *Int. J. Comput. Vis.* 123, 32–73.
- [20] Li, B., Wang, R., Wang, G., Ge, Y., Ge, Y., Shan, Y., 2023a. Seed-bench: Benchmarking multimodal llms with generative comprehension. *CoRR abs/2307.16125*.
- [21] Li, B., Zhang, Y., Guo, D., Zhang, R., Li, F., Zhang, H., Zhang, K., Li, Y., Liu, Z., Li, C., 2024. Llava-onevision: Easy visual task transfer. *CoRR abs/2408.03326*.
- [22] Li, J., Li, D., Savarese, S., Hoi, S.C.H., 2023b. BLIP-2: bootstrapping language-image pre-training with frozen image encoders and large language models, in: ICML, PMLR. pp. 19730–19742.
- [23] Li, Y., Du, Y., Zhou, K., Wang, J., Zhao, W.X., Wen, J., 2023c. Evaluating object hallucination in large vision-language models, in: EMNLP, Association for Computational Linguistics. pp. 292–305.
- [24] Lin, J., Yin, H., Ping, W., Molchanov, P., Shoeybi, M., Han, S., 2024. VILA: on pre-training for visual language models, in: CVPR, IEEE. pp. 26679–26689.
- [25] Liu, F., Emerson, G., Collier, N., 2023a. Visual spatial reasoning. *Trans. Assoc. Comput. Linguistics* 11, 635–651.
- [26] Liu, H., Li, C., Li, Y., Lee, Y.J., 2024a. Improved baselines with visual instruction tuning, in: CVPR, IEEE. pp. 26286–26296.
- [27] Liu, H., Li, C., Wu, Q., Lee, Y.J., 2023b. Visual instruction tuning, in: NeurIPS.
- [28] Liu, H., Xue, W., Chen, Y., Chen, D., Zhao, X., Wang, K., Hou, L., Li, R., Peng, W., 2024b. A survey on hallucination in large vision-language models. *CoRR abs/2402.00253*.
- [29] Liu, Y., Duan, H., Zhang, Y., Li, B., Zhang, S., Zhao, W., Yuan, Y., Wang, J., He, C., Liu, Z., Chen, K., Lin, D., 2024c. Mmbench: Is your multi-modal model an all-around player?, in: ECCV (6), Springer. pp. 216–233.
- [30] Lu, P., Bansal, H., Xia, T., Liu, J., Li, C., Hajishirzi, H., Cheng, H., Chang, K., Galley, M., Gao, J., 2024. Mathvista: Evaluating mathematical reasoning of foundation models in visual contexts, in: ICLR, OpenReview.net.
- [31] Lu, P., Mishra, S., Xia, T., Qiu, L., Chang, K., Zhu, S., Tafjord, O., Clark, P., Kalyan, A., 2022. Learn to explain: Multimodal reasoning via thought chains for science question answering, in: NeurIPS.
- [32] Mao, J., Huang, J., Toshev, A., Camburu, O., Yuille, A.L., Murphy, K., 2016. Generation and comprehension of unambiguous object descriptions, in: CVPR, IEEE Computer Society. pp. 11–20.

- [33] McKinzie, B., Gan, Z., Fauconnier, J., Dodge, S., Zhang, B., Dufter, P., Shah, D., Du, X., Peng, F., Belyi, A., Zhang, H., Singh, K., Kang, D., Hè, H., Schwarzer, M., Gunter, T., Kong, X., Zhang, A., Wang, J., Wang, C., Du, N., Lei, T., Wiseman, S., Lee, M., Wang, Z., Pang, R., Gräsch, P., Toshev, A., Yang, Y., 2024. MM1: methods, analysis and insights from multimodal LLM pre-training, in: ECCV (29), Springer. pp. 304–323.
- [34] Mishra, A., Shekhar, S., Singh, A.K., Chakraborty, A., 2019. OCR-VQA: visual question answering by reading text in images, in: ICDAR, IEEE. pp. 947–952.
- [35] OpenAI, 2024. A primer on sports analytics: A new dimension of sports. <https://openai.com/index/hello-gpt-4o/>.
- [36] Sanders, S., 2015. How do you like los angeles’ new parking signs? URL: <https://www.npr.org/sections/thetwo-way/2015/04/06/397858800/how-do-you-like-los-angeles-new-parking-signs>.
- [37] Schwenk, D., Khandelwal, A., Clark, C., Marino, K., Mottaghi, R., 2022. A-OKVQA: A benchmark for visual question answering using world knowledge, in: ECCV (8), Springer. pp. 146–162.
- [38] Tong, S., II, E.L.B., Wu, P., Woo, S., IYER, A.J., Akula, S.C., Yang, S., Yang, J., Middepogu, M., Wang, Z., Pan, X., Fergus, R., LeCun, Y., Xie, S., 2024. Cambrian-1: A fully open, vision-centric exploration of multimodal LLMs, in: The Thirty-eighth Annual Conference on Neural Information Processing Systems. URL: <https://openreview.net/forum?id=Vi8AepAXGy>.
- [39] Vaswani, A., Shazeer, N., Parmar, N., Uszkoreit, J., Jones, L., Gomez, A.N., Kaiser, L., Polosukhin, I., 2017. Attention is all you need, in: NIPS, pp. 5998–6008.
- [40] Wang, P., Bai, S., Tan, S., Wang, S., Fan, Z., Bai, J., Chen, K., Liu, X., Wang, J., Ge, W., Fan, Y., Dang, K., Du, M., Ren, X., Men, R., Liu, D., Zhou, C., Zhou, J., Lin, J., 2024. Qwen2-vl: Enhancing vision-language model’s perception of the world at any resolution. CoRR abs/2409.12191.
- [41] Wu, Z., Chen, X., Pan, Z., Liu, X., Liu, W., Dai, D., Gao, H., Ma, Y., Wu, C., Wang, B., Xie, Z., Wu, Y., Hu, K., Wang, J., Sun, Y., Li, Y., Piao, Y., Guan, K., Liu, A., Xie, X., You, Y., Dong, K., Yu, X., Zhang, H., Zhao, L., Wang, Y., Ruan, C., 2024. Deepseek-vl2: Mixture-of-experts vision-language models for advanced multimodal understanding. URL: <https://arxiv.org/abs/2412.10302>, arXiv:2412.10302.
- [42] xAI, 2024. Realworldqa. URL: <https://x.ai/blog/grok-1.5v>.
- [43] Xing, Y., Li, Y., Laptev, I., Lu, S., 2024. Mitigating object hallucination via concentric causal attention, in: The Thirty-eighth Annual Conference on Neural Information Processing Systems. URL: <https://openreview.net/forum?id=CIRPE1bSmV>.
- [44] Xue, L., Shu, M., Awadalla, A., Wang, J., Yan, A., Purushwalkam, S., Zhou, H., Prabhu, V., Dai, Y., Ryoo, M.S., Kendre, S., Zhang, J., Qin, C., Zhang, S., Chen, C., Yu, N., Tan, J., Awalgaonkar, T.M., Heinecke, S., Wang, H., Choi, Y., Schmidt, L., Chen, Z., Savarese, S., Niebles, J.C., Xiong, C., Xu, R., 2024. xgen-mm (BLIP-3): A family of open large multimodal models. CoRR abs/2408.08872.
- [45] Yao, Y., Yu, T., Zhang, A., Wang, C., Cui, J., Zhu, H., Cai, T., Li, H., Zhao, W., He, Z., Chen, Q., Zhou, H., Zou, Z., Zhang, H., Hu, S., Zheng, Z., Zhou, J., Cai, J., Han, X., Zeng, G., Li, D., Liu, Z., Sun, M., 2024. Minicpm-v: A GPT-4V level MLLM on your phone. CoRR abs/2408.01800.
- [46] Yin, S., Fu, C., Zhao, S., Li, K., Sun, X., Xu, T., Chen, E., 2023. A survey on multimodal large language models. CoRR abs/2306.13549.
- [47] You, H., Zhang, H., Gan, Z., Du, X., Zhang, B., Wang, Z., Cao, L., Chang, S., Yang, Y., 2024. Ferret: Refer and ground anything anywhere at any granularity, in: ICLR, OpenReview.net.
- [48] Yu, L., Poirson, P., Yang, S., Berg, A.C., Berg, T.L., 2016. Modeling context in referring expressions, in: ECCV (2), Springer. pp. 69–85.

- [49] Yu, W., Yang, Z., Li, L., Wang, J., Lin, K., Liu, Z., Wang, X., Wang, L., 2024. Mm-vet: Evaluating large multimodal models for integrated capabilities, in: ICML, OpenReview.net.
- [50] Yue, X., Ni, Y., Zheng, T., Zhang, K., Liu, R., Zhang, G., Stevens, S., Jiang, D., Ren, W., Sun, Y., Wei, C., Yu, B., Yuan, R., Sun, R., Yin, M., Zheng, B., Yang, Z., Liu, Y., Huang, W., Sun, H., Su, Y., Chen, W., 2024. MMMU: A massive multi-discipline multimodal understanding and reasoning benchmark for expert AGI, in: CVPR, IEEE. pp. 9556–9567.
- [51] Zhai, X., Mustafa, B., Kolesnikov, A., Beyer, L., 2023. Sigmoid loss for language image pre-training, in: ICCV, IEEE. pp. 11941–11952.
- [52] Zhang, H., Gao, M., Gan, Z., Dufter, P., Wenzel, N., Huang, F., Shah, D., Du, X., Zhang, B., Li, Y., Dodge, S., You, K., Yang, Z., Timofeev, A., Xu, M., Chen, H., Fauconnier, J., Lai, Z., You, H., Wang, Z., Dehghan, A., Grasch, P., Yang, Y., 2024. MM1.5: methods, analysis & insights from multimodal LLM fine-tuning. CoRR abs/2409.20566.
- [53] Zhu, D., Chen, J., Shen, X., Li, X., Elhoseiny, M., 2024. Minigpt-4: Enhancing vision-language understanding with advanced large language models, in: ICLR, OpenReview.net.

Configurations	Pre-Training	Supervised Finetuning
Vision Encoder	siglip-so400m-patch14-384	
VL-Connector	Perceiver Resampler	
LLM	Phi-3.5-mini-instruct	
Trainable Modules	VL-Connector, LLM	
# Visual tokens	144	
Batch Size	192	64
Learning Rate	1e-4	2e-5
Minimum LR	1e-5	1e-6
LR Schedule	Cosine Decay	
Warmup Steps	2000	150
Training Steps	50k (Sec. 4.2)/275k (AKI)	5k (Sec. 4.2)/10k (AKI)
Weight Decay	1e-2	1e-4
Optimizer	AdamW	
Gradient Clipping	1.0	
Precision	amp_bf16	
Max Length	128	512

Table 3: Hyperparameters for pretraining and finetuning experiments in Section 4.2 and for our AKI model.

Task	Dataset	Total Size	Sampling Probability
Open-ended VQA	VQAv2	83k	10.3%
	GQA	72k	10.3%
	VSR	8k	2.6%
	OCRVQA	80k	10.3%
Multi-choices VQA	A-OKVQA	50k	10.3%
	ScienceQA	12k	10.3%
Referring expression	RefCOCO	120k	10.3%
	RefCOCOG	80k	10.3%
	RefCOCO+	120k	10.3%
	VisualGnome	86k	4.7%
Instruction-following	LLaVA-150k	158k	10.3%

Table 4: Statistics for supervised finetuning datasets.

Appendix

A Implementation Details

In this section, we provide detailed settings for our implementations, training configurations, as well as the prompt template.

A.1 Hyper-Parameter Settings

Our implementation is built on PyTorch with Fully Sharded Data Parallel (FSDP), leveraging the OpenFlamingo codebase³. To enhance computational efficiency and optimize throughput, we employ PyTorch’s Automatic Mixed Precision (AMP) with bfloat16, which allows for reduced memory usage while maintaining numerical stability. A comprehensive summary of the hyperparameters used in our experiments is provided in Table 3.

For model training, we conducted experiments on a single node equipped with $8 \times$ A100 (80GB) GPUs. The training duration varied depending on the model configuration: Each model in Section 4.2 required approximately 2 days for pretraining and 1 day for supervised finetuning. The AKI-4B model, given its larger scale, required around 3 weeks for pretraining and 2 days for supervised

³https://github.com/mlfoundations/open_flamingo

Task	Dataset	Prompt Template
Pre-Training Template		
Captioning	BLIP3-KALE	<image>{image_tokens}{caption}<endofchunk>
Supervised Finetuning Template		
System Message: <systeml> A chat between a curious user and an artificial intelligence assistant. The assistant gives helpful, detailed, and polite answers to the user’s questions. <endl>		
Open-ended VQA	VQAv2 GQA VSR OCRvQA	{system message} <userl> <image> {image_tokens} Answer the question using a single word or phrase. {question}<endl> <assistantl> {answer}
Multi-choices VQA	A-OKVQA ScienceQA	{system message} <userl> <image> {image_tokens} Answer with the option’s letter from the given choices directly. {question} Options: {options} <endl> <assistantl> {answer}
Referring expression	RefCOCO RefCOCog RefCOCO+ VisualGnome	{system message} <userl> <image> {image_tokens} Provide a short description for this region. <bbox>{bbox}</bbox> <endl> <assistantl> {answer}
Instruction-following	LLaVA-150k	{system message} <userl> <image> {image_tokens} {question} <endl> <assistantl> {answer}

Table 5: Detailed prompt template for each dataset. The templates are mainly followed [9, 27]. {system message} in each dataset template is replaced with the system message. {image_tokens}, {questions}, and {answer} are replaced based on each data sample. The bounding box coordinates {bbox} are normalized as $[x_{min}, y_{min}, x_{max}, y_{max}]$.

finetuning. For all benchmark evaluations, we employed greedy decoding to generate responses, ensuring consistency across different models and datasets.

For supervised finetuning, we adopt a sampling ratio for the collected dataset similar to [9], as detailed in Table 4. To assess the impact of different sampling strategies, we empirically compared this hand-crafted ratio with a random ratio, where each data sample is selected based on a uniform distribution. Our findings indicate that using the hand-crafted ratio results in slightly better performance compared to the random ratio, suggesting that a carefully balanced dataset composition contributes to improved multimodal learning. Specifically, VQAv2, GQA, OCRvQA, A-OKVQA, ScienceQA, RefCOCO, RefCOCog, RefCOCO+, and LLaVA-150k each have an equal sampling ratio of 10.3%. VSR is assigned a lower sampling ratio of 2.6%, reflecting its unique task characteristics. VisualGnome is set at 4.7%, as it contains most samples.

A.2 Prompt Templates

To ensure the reproducibility of our model, we provide detailed dataset templates for both the pretraining and supervised finetuning stages in Table 5. For pretraining, we follow the template format introduced in [5], structured as:

$$\text{<image>}\{image_tokens\}\{caption\}\text{<endofchunk|>}, \tag{7}$$

where image tokens are followed by the caption, and <endofchunk|> is used as a boundary marker.

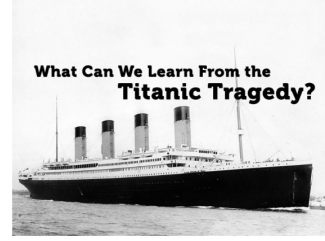
For supervised finetuning, we adopt the dataset templates from [9], with the exception of the referring expression tasks (RefCOCO, RefCOCog, RefCOCO+, and VisualGnome). Instead, we employ the



In the provided image, a John Deere tractor attachment from 1991 is depicted. The attachment features a large wheel in the foreground, encircled by a yellow rim. The logo of a leaping deer in black and white adorns the center. Surrounding the attachment are other green tractors and machinery, while the ground consists of a mixture of gravel and dirt. The overcast sky indicates a cloudy day.

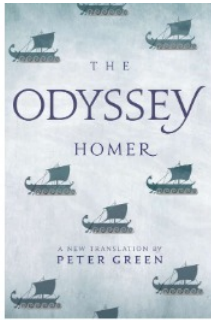


In the enchanting forest of Moldova, depicted in the image, the sun's rays filter through the dense canopy during either dawn or dusk, casting a warm, golden hue over the landscape. The forest floor is adorned with a rich layer of fallen leaves, and a narrow path weaves through the scene, inviting exploration. The ancient trees, with their twisted and gnarled trunks, testify to the forest's enduring history, adding to the overall ambiance of tranquility and mystery.



The RMS Titanic, a renowned ocean liner that met its tragic end in 1912, is depicted in this black-and-white photograph. With four large smokestacks gracing its deck, the ship is shown amidst the water's expanse, displaying an apparent motion that stirs the surrounding waves. Reflecting on this maritime disaster, we ask: What Can We Learn From the Titanic Tragedy?

Figure 6: Illustrations sampled from the Blip3-kale dataset.



The image contains the text "THE", the text "ODYSSEY", the text "HOMER", the text "A NEW TRANSLATION BY", the text "PETER GREEN"



The image contains the text "GEORGE'S"



The image contains the text "MOVEMENT"

Figure 7: Illustrations sampled from the Blip3-OCR dataset.

template with “Provide a short description for this region.” following [27] based on our empirical experiments. Additionally, we do not apply de-duplication techniques in data processing. Multi-turn dialogues are converted into multiple single-turn samples, ensuring consistency across different datasets.

B Dataset Details

In this section, we provide a brief overview of the key aspects for each dataset we use for pretraining and supervised finetuning.

B.1 Pretraining Data

We adopt Blip3-kale [6] and Blip3-ocr-200m [44] as the pretraining datasets. Blip3-kale consists of 218M image-text captions by augmenting synthetic dense image captions with web-scale to generate factually grounded image captions, where the images are originally come from the Datacomp-1B dataset [15]. The Blip3-OCR-200M dataset comprises 12 hierarchical levels, ranging from coarse to fine-grained representations for text-rich images. We utilize Level 1 (basic text extraction) to enhance the model’s ability to recognize and interpret text within images. For Blip3-Kale, approximately 10 million and 100 million captioning pairs were sampled for the experiments in Section 4.2 and the final AKI-4B model, respectively. Additionally, around 5 million samples from Blip3-OCR-200M were used to train the AKI-4B model. Some examples sampled from the Blip3-kale and Blip3-ocr-200m datasets are provided in Figures 6 and 7, respectively.

B.2 Supervised Finetuning Data

Generally, the aim of supervised finetuning is to enable the model to learn specific skills from related domains (e.g., VQA). Since the main focus in this paper is to improve multimodal performance from the fundamental architecture perspective, instead of from scaling numbers of datasets and parameters like Cambrian and QWen, we mainly use VQA and referring expression datasets as our visual instruction tuning datasets. Specifically, the brief introduction of each dataset is describe as follows:

- **VQA_{v2} [16]:** A large-scale Visual Question Answering dataset containing images paired with open-ended questions and human-annotated answers from various capabilities, e.g., visual grounding, spatial understanding, visual recognition.
- **GQA [17]:** is a scene understanding dataset featuring compositional questions over real-world images, including semantic representations of the scenes and questions to mitigate language priors and conditional biases for different question types.
- **VSR [25]:** is a visual spatial reasoning dataset containing text-image pairs with various types of spatial relations in English (e.g., under, in front of), which is an important criteria for multimodal understanding.
- **OCRVQA [34]:** learns the ability of the VQA task that interprets text in images, which is often known as the OCR capability.
- **A-OKVQA [37]:** aspires to provide the requirement of understanding form of commonsense reasoning about the image. The questions in A-OKVQA generally cannot be answered by simply querying a knowledge base.
- **ScienceQA [31]:** consists of image-text multiple choice questions with diverse science topics, including annotations of their answers with corresponding lectures and explanations.
- **RefCOCO [18]:** A dataset for referring expression comprehension, where a model must localize a specific object in an image given a natural language description, collected from interactive games.
- **RefCOCOg [32]:** A variation of RefCOCO with longer and more descriptive referring expressions, supporting more complex reasoning.
- **RefCOCO+ [48]:** A referring expression comprehension dataset like RefCOCO but focusing on descriptions without absolute location words, making localization more challenging.
- **VisualGnome [19]:** contains densely annotated region descriptions, VQA, object instances, attributes, and relationships, aiming to connect structured image concepts to language.
- **LLaVA-150k [27]:** is a GPT-generated dataset for learning multimodal instruction-following capabilities. Its aim is to enable the model towards the multimodal capability of GPT-4.

C Benchmark Details

In this section, we provide detailed descriptions of the evaluations conducted in the experiments, including the prompt templates as well as comprehensive metric results for each benchmark.

C.1 Prompt Template for Benchmark Evaluations

Table 6 presents the detailed prompt templates used for evaluating each multimodal benchmark to ensure reproducibility. For clarity, we omit the system messages and special tokens, following the format in Table 5. Furthermore, for benchmarks such as MMB and MathV^{mini}, hints are included only when explicitly provided in the sample.

C.2 Detailed Benchmark Scores

Beyond demonstrating the effectiveness of our approach, we provide detailed metrics for each evaluation benchmark to offer deeper insights into both the strengths and limitations across different categories from Tables 7 to 15. We believe that sharing comprehensive results can contribute to

Benchmark	Prompt Template
MME ^{PIC}	Answer the question using a single word or phrase. {question} Please answer yes or no.
MMB ^{dev}	Answer with the option’s letter from the given choices directly. Hint: {hint}\n Question: {question}\n Options: {options}
SEED ^I	Answer with the option’s letter from the given choices directly. {question}\n Options: {options}
LLaVA ^W	{question}
MMMU	Answer with the option’s letter from the given choices directly. {question}\n Options: {options}
MathV ^{mini}	Hint: {hint}\n Question: {question}
POPE	Answer the question using a single word or phrase. {question} Please answer yes or no.
MM-Vet	{question}
RealWorldQA	Answer with the option’s letter from the given choices directly. {question}\n Options: {options}
CV-Bench ^{2D/3D}	Answer with the option’s letter from the given choices directly. {question}\n Options: {options}

Table 6: Detailed prompt template for evaluating each benchmark. We omit the system message and special tokens for better readability as in Table 5. The hint in MMB and MathV^{mini} is included only if provided.

Model	(I&T) _{PT} + (I&T) _{SFT}	CCA		DOT (Ours)	MMA (Ours)		🇨🇦 AKI-4B
Perception							
OCR	57.5	70		65	80		132.5
Artwork	133.5	131		140	135		126.8
Celebrity	109.1	72.4		111.5	122.9		124.1
Color	138.3	145		150	163.3		163.3
Count	98.3	130		133.3	148.3		175
Existence	145	165		165	175		195
Landmark	140.5	149.5		143.3	149.8		154.3
Position	96.7	81.7		81.7	90		111.7
Posters	145.6	119.4		120.1	123.8		151
Scene	161.8	148.5		158	156.8		158.3
Sum	1226.3	1212.7		1267.8	1344.9		1491.9
Cognition							
Code reasoning	50	62.5		50	52.5		55
Commonsense reasoning	105.7	93.6		101.4	117.9		117.9
Numerical calculation	40	40		42.5	52.5		50
Text translation	62.5	47.5		57.5	92.5		140
Sum	258.2	243.6		251.4	315.4		362.9

Table 7: Detailed perception and cognition scores for MME, with a maximum score of 200 for each category (row).

advancing multimodal understanding. For benchmarks requiring LLM-based evaluation (e.g., MM-Vet), we use GPT-4-0613 as the judgment grader. Additionally, certain benchmarks are excluded from the detailed breakdown since they rely on a single metric (e.g., RealWorldQA).

D Qualitative Results

In addition to the quantitative results, we further analyze the qualitative outputs generated by the baselines ((I&T)_{PT} + (I&T)_{SFT}) and CCA, as well as our proposed MMA method. Figures 8, 9, 10, and 11 present samples from various multimodal benchmarks, including multiple-choice and open-ended questions. The comparisons between the baseline and CCA reveal that while CCA reduces hallucinations in the multiple-choice case (Figure 8), it still generates responses containing hallucinated objects (e.g., both Figures 9 and 11). Moreover, CCA produces an unrelated response



User: Where is the water compared to the tater tots?
 A. The water is behind to the right of the tater tots.
 B. The water is in front to the right of the tater tots.
 C. The water is behind to the left of the tater tots.

(I&T)_{PT} + (I&T)_{SFT}: B

CCA: A

MMA (Ours): A

Figure 8: Qualitative comparisons among the conventional training pipeline ((I&T)_{PT} + (I&T)_{SFT}), CCA, and our MMA method. The sample is taken from RealWorldQA [42].



User: What fruit is the the right of plums?

(I&T)_{PT} + (I&T)_{SFT}: apple

CCA: strawberries

MMA (Ours): oranges

Figure 9: Qualitative comparisons among the conventional training pipeline ((I&T)_{PT} + (I&T)_{SFT}), CCA, and our MMA method. The sample is taken from MM-Vet [49].



User: What are all the scene text in the image?

(I&T)_{PT} + (I&T)_{SFT}: s 3002 cdd

CCA: all the scene text in the image are the license plate

MMA (Ours): s3302cd

Figure 10: Qualitative comparisons among the conventional training pipeline ((I&T)_{PT} + (I&T)_{SFT}), CCA, and our MMA method. The sample is taken from MM-Vet [49].



User: What is the brand of the yogurt flavored with blueberry?

(I&T)_{PT} + (I&T)_{SFT}: The brand of the yogurt is yogurt.

CCA: The brand of the yogurt is tropicana.

MMA (Ours): The brand of the yogurt is Fage.

Figure 11: Qualitative comparisons among the conventional training pipeline ((I&T)_{PT} + (I&T)_{SFT}), CCA, and our MMA method. The sample is taken from LLaVA^w [27].

Model	AR	CP	FP-C	FP-S	LR	RR	Overall
(I&T) _{PT} + (I&T) _{SFT}	75.6	71.0	53.1	70.2	34.7	66.7	64.9
CCA	78.0	73.2	59.2	73.0	34.7	67.8	67.4
DOT (Ours)	56.1	53.9	27.4	46.0	21.0	40.8	43.8
MMA (Ours)	75.9	78.0	63.6	71.7	48.3	67.8	70.3
🇨🇦 AKI-4B	76.8	81.1	66.0	75.7	46.9	0.65	73.1

Table 8: Detailed scores (%) for MMB. Abbreviations: AR – Attribute Reasoning, CP – Coarse Perception, FP-C – Fine-grained Perception (cross-instance), FP-S – Fine-grained Perception (single-instance), LR – Logical Reasoning, RR – Relation Reasoning.

Model	(I&T) _{PT} + (I&T) _{SFT}	CCA	DOT (Ours)	MMA (Ours)	🇨🇦 AKI-4B
Instance attributes	64.1	66.6	53.7	69.5	69.5
Instance identity	68.5	69.9	58.4	70.6	69.2
Instance interaction	64.9	61.9	59.8	72.2	64.1
Instance location	55.7	55.2	45.7	56.4	55.7
Instance counting	56.7	56.3	45.1	59.4	58.7
Scene understanding	72.9	73.9	66.9	74.6	76.8
Spatial relation	46.7	50.2	39.9	48.9	47.2
Text understanding	36.9	35.7	25.0	31.0	34.6
Visual reasoning	77.0	76.1	66.5	75.5	75.9
Overall	64.1	65.3	54.7	67.1	69.4

Table 9: Detailed accuracy for each category in SEED¹.

in text-rich understanding tasks (e.g., Figure 10), whereas the baseline at least identifies the correct direction, albeit with incorrect details. In contrast, our MMA method effectively mitigates these issues across both multiple-choice and open-ended questions, demonstrating its ability to enhance response accuracy and coherence.


Model	Conv	Detail	Complex	Total
(I&T) _{PT} + (I&T) _{SFT}	24.1	59.7	55.0	47.0
CCA	33.3	60.7	63.6	54.0
DOT (Ours)	29.8	53.0	58.5	47.5
MMA (Ours)	38.6	61.9	71.7	59.6
 AKI-4B	91.1	57.4	73.4	74.6

Table 10: Detailed scores for LLaVA^W.


Model	(I&T) _{PT} + (I&T) _{SFT}	CCA	DOT (Ours)	MMA (Ours)	 AKI-4B
Accounting	60	27	20	40	40
Agriculture	20	40	0	20	0
Architecture & Engineering	0	40	20	0	0
Art	40	50	20	40	20
Art theory	40	57	20	20	40
Basic medical science	60	37	80	60	40
Biology	60	27	20	60	60
Chemistry	40	13	20	20	40
Clinical medicine	40	47	40	0	20
Computer science	40	30	20	40	40
Design	40	43	40	40	40
Diagnostics & Laboratory medicine	40	23	20	0	40
Economics	40	47	40	80	60
Electronics	20	40	20	20	40
Energy & Power	20	30	40	60	60
Finance	0	20	0	40	0
Geography	0	40	20	20	20
History	40	37	60	60	60
Literature	60	70	40	60	60
Manage	40	27	20	60	40
Marketing	40	23	20	40	80
Materials	40	20	40	20	0
Math	20	33	40	40	20
Mechanical engineering	0	30	0	0	40
Music	20	43	40	20	40
Pharmacy	20	40	60	40	40
Physics	20	20	20	80	60
Psychology	20	23	40	60	40
Public health	20	23	20	20	60
Sociology	60	43	80	60	60
Art & Design	35	48	30	30	35
Business	36	29	20	52	44
Health & Medicine	36	34	44	24	40
Humanities & Social science	45	43	55	60	55
Science	28	27	24	44	40
Tech & Engineering	20	32	20	23	26
Overall	31	35	31	37	39

Table 11: Detailed accuracy (%) of each category for MMMU.

	(I&T) _{PT} + (I&T) _{SFT}	CCA		DOT (Ours)	MMA (Ours)	🇨🇦AKI-4B
Scientific reasoning	34.4	38.5		36.9	37.7	38.5
Textbook QA	34.8	38.6		38.6	36.1	44.3
Numeric commonsense	19.4	20.1		16.7	20.8	27.8
Arithmetic reasoning	21.3	27.2		24.9	29.8	27.5
VQA	21.2	33.0		30.2	36.9	42.5
Geometry reasoning	19.7	16.3		20.5	18.0	26.4
Algebraic reasoning	24.2	20.6		23.1	20.6	24.9
Geometry problem solving	21.2	16.8		21.1	18.8	23.6
Math word problem	12.9	20.4		18.3	21.5	15.6
Logical reasoning	10.8	16.2		21.6	16.2	10.8
Figure QA	23.4	23.4		23.4	23.1	28.6
Statistical reasoning	22.3	22.6		23.6	22.9	27.9
Total	24.2	25.6		25.6	26.4	32.1

Table 12: Detailed scores for different skills in MathV^{mini}.

Model	Split	Accuracy	Precision	Recall		Overall
(I&T) _{PT} + (I&T) _{SFT}	Popular	82.3	92.6	70.1		79.8
	Adversarial	80.7	88.9	70.1		78.4
	Random	83.8	96.4	70.1		81.2
	Overall	82.2	92.6	70.1		79.8
CCA	Popular	84.5	95.8	72.1		82.3
	Adversarial	82.9	92.0	72.1		80.8
	Random	84.9	97.0	72.1		82.7
	Overall	84.1	94.9	72.1		81.9
DOT (Ours)	Popular	82.5	84.1	74.6		82.5
	Adversarial	82.9	89.4	74.6		81.4
	Random	86.0	96.6	74.6		84.2
	Overall	84.3	92.7	74.6		82.7
MMA (Ours)	Popular	84.7	95.2	73.1		82.7
	Adversarial	83.7	92.7	73.1		81.7
	Random	85.7	97.8	73.1		83.7
	Overall	84.7	95.2	73.1		82.7
🇨🇦AKI-4B	Popular	87.4	90.8	83.3		86.9
	Adversarial	84.8	85.9	83.3		84.6
	Random	90.0	96.2	83.3		89.3
	Overall	87.4	90.8	83.3		86.9

Table 13: Accuracy, precision, and recall on the popular, adversarial, and random splits for POPE.

Model	rec	ocr	know	gen	spat	math		Overall
(I&T) _{PT} + (I&T) _{SFT}	36.4	17.5	11.4	10.7	18.0	0.0		24.3
CCA	40.5	19.3	18.2	14.7	26.0	3.85		29.0
DOT (Ours)	34.6	17.8	9.9	5.6	27.6	9.6		25.0
MMA (Ours)	39.8	22.1	20.5	16.6	27.5	3.8		30.1
🇨🇦AKI-4B	48.2	36.1	22.6	21.4	36.1	23.1		40.8

Table 14: Detailed scores across different categories for MM-Vet.


Model	ADE20k	COCO	Omni3D		2D Acc.	3D Acc.
(I&T) _{PT} + (I&T) _{SFT}	41.2	49.2	54.3		45.2	54.3
CCA	48.0	64.0	62.8		56.0	62.8
DOT (Ours)	47.2	57.1	58.1		52.2	58.1
MMA (Ours)	52.9	62.7	64.1		57.8	64.1
 AKI-4B	60.6	63.6	71.8		62.1	71.8

Table 15: Accuracy of each source for CV-Bench.